AD-A234 746

(2)

TECHNICAL REPORT NO. 18

To

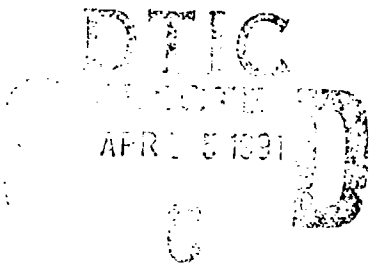

The Office of Naval Research
Contract No. N00014-86-K-0381

ADVANCED PROCESSING AND PROPERTIES OF HIGH PERFORMANCE ALLOYS

D. A. Koss

Department of Materials Science and Engineering
The Pennsylvania State University
University Park, PA 16802

Final Report for the period 1 May 1986 - November 30, 1990

Reproduction in Whole or in Part is Permitted
For Any Purpose of the United States Government
Distribution of this Document is Unlimited

DTIC FILE COPY

91 4 12 039

SECURITY CLASSIFICATION OF THIS PAGE

REPORT DOCUMENTATION PAGE

Form Approved OMB No 0704-0188

1a REPORT SECURITY CLASSIFICATION: Unclassified	1b RESTRICTIVE MARKINGS
2a SECURITY CLASSIFICATION AUTHORITY	3 DISTRIBUTION/AVAILABILITY OF REPORT: Distribution of this document is unlimited
2b DECLASSIFICATION/DOWNGRADING SCHEDULE	
4 PERFORMING ORGANIZATION REPORT NUMBER(S): Technical Report No. 18	5 MONITORING ORGANIZATION REPORT NUMBER(S)
6a NAME OF PERFORMING ORGANIZATION; 6b OFFICE SYMBOL (If applicable)	7a NAME OF MONITORING ORGANIZATION
6c ADDRESS (City, State, and ZIP Code): Dept. of Materials Science & Engineering, The Penn. State University, University Park, PA 16802	7b ADDRESS (City, State, and ZIP Code)
8a NAME OF FUNDING/SPONSORING ORGANIZATION: Office of Naval Research; 8b OFFICE SYMBOL (If applicable)	9 PROCUREMENT INSTRUMENT IDENTIFICATION NUMBER: N00014-86-K-0381
8c ADDRESS (City, State, and ZIP Code): Office of Naval Research, Code 1131, 800 N. Quincy Street, Arlington, VA 22217	10 SOURCE OF FUNDING NUMBERS: PROGRAM ELEMENT NO; PROJECT NO; TASK NO; WORK UNIT ACCESSION NO.
11 TITLE (Include Security Classification): Advanced Processing and Properties of High Performance Alloys	
12 PERSONAL AUTHOR(S)	
13a TYPE OF REPORT: Final; 13b TIME COVERED FROM 5/1/86 TO 11/30/90	14 DATE OF REPORT (Year, Month, Day): April 4, 1991; 15 PAGE COUNT: 32
16 SUPPLEMENTARY NOTATION	

17 COSATI CODES			18 SUBJECT TERMS (Continue on reverse if necessary and identify by block number)		
FIELD	GROUP	SUB GROUP	Porosity	Low Cycle Fatigue	Cu-Nb alloys
			Voids	Ti Alloys	Rapid Solidificati
			Fracture	Strain-Path Effects	

19 ABSTRACT (Continue on reverse if necessary and identify by block number)

Progress is reviewed for a research program whose purpose was to establish a broad-based understanding of the application and consequences of advanced processing techniques, especially as they influence the strength and fracture resistance of high performance structural alloys. The research areas are as follows: (1) the mechanism of strain-induced void/pore linking during ductile fracture, (2) the influence of porosity of low cycle fatigue, (3) processing and proprieties of Cu-Nb alloys, (4) the deformation of rapidly solidified Ti alloys at elevated temperatures, (5) strain-path effects on fracture, and (6) a new age-hardenable beta titanium alloy.

20 DISTRIBUTION/AVAILABILITY OF ABSTRACT: ☒ UNCLASSIFIED/UNLIMITED ☐ SAME AS RPT ☐ DTIC USERS	21 ABSTRACT SECURITY CLASSIFICATION
22a NAME OF RESPONSIBLE INDIVIDUAL: Donald A. Koss	22b TELEPHONE (Include Area Code): 814-865-5447; 22c OFFICE SYMBOL

DD Form 1473, JUN 86 Previous editions are obsolete SECURITY CLASSIFICATION OF THIS PAGE

S/N 0102-LF-014-6603

ADVANCED PROCESSING AND PROPERTIES OF HIGH PERFORMANCE ALLOYS

INTRODUCTION

Advanced structural systems require a new generation of high performance materials which exhibit dramatic improvements in both strength and fracture resistance over a wide range of temperatures and environments. With such materials becoming increasingly dependent on advanced processing techniques, a fundamental problem has developed: the rate of application of new processing methods exceeds the basic knowledge base necessary to anticipate fully the resulting behavior of the component in service. Thus, while novel alloy microstructures are created through advanced processing techniques, the promise of improved properties is usually accompanied by the potential for a new set of problems. For instance, rapidly solidified dispersion- hardened alloys may exhibit superior short time tensile strengths but inadequate high temperature creep strength due to the stabilization of fine grain sizes and the resulting enhanced grain boundary sliding. As a result, despite notable improvements in some aspects of a material's properties, in-service reliability may be impaired, especially if computational methods to make accurate life prediction are lacking.

The primary purpose of this research was to provide a broad-based understanding of the applications and consequences of certain advanced processing techniques used to create new high performance alloys. The research was wide ranging in scope and included fundamental studies of the mechanisms of void or pore linking during ductile fracture, the influence of porosity on low cycle fatigue, as well as processing-property relationships in Cu-Nb alloys. The present report summarizes progress in the areas of research for the period 5/1/86 to 11/30/90 performed under the auspices of Contract No. N00014-86-D-0381. The research areas are as follows:

(1) the mechanism of strain-induced void/pore linking during ductile fracture,

(2) the influence of porosity of low cycle fatigue,

(3) processing and properties of Cu-Nb alloys,

(4) the deformation of rapidly solidified Ti alloys at elevated temperatures,

(5) strain-path effects on fracture, and

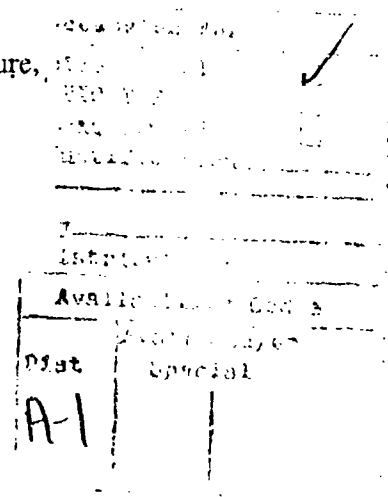

(6) a new age-hardenable beta titanium alloy.

A significant impact of the above research is the educational experience derived by the graduate students involved. The following students have been a part of the ONR program during the period cited: Stephen Kampe, Ph.D., January 1987; Paul Magnusen, Ph.D. July, 1987; Susan Kestner, M.S., May, 1986; Dale Gerard, Ph.D., November, 1988; Kevin Zeik, Ph.D. candidate; Andrew Geltmacher, M.S., December, 1990, currently Ph.D. candidate, and Louis Quattrocchi, M.S. candidate.

SUMMARY OF RESEARCH

1. The Mechanism of Strained-Induced Void/Pore Linking During Ductile Fracture
[with Paul Magnusen, Ph.D., and Andrew Geltmacher, M.S., currently Ph.D. candidate]

The presence of pre-existing porosity and the subsequent processes of pore linking during deformation is known to have a strong effect on the ductile fracture of porous materials (see for example, ref. 1). Similarly, strain-induced void linking is a integral part of the ductile fracture process. Although differing in their origin, pores and voids link is a similar manner during low temperature deformation, and thus failure of a porous or "voided" material may be examined together in a single analysis. Although void/pore linking is a very important step in the process of ductile fracture, its physical basis has not been properly understood until our recent studies[2-4] The reason for this situation is that nearly all of the previous work on void/pore growth and linking assumed regular arrays of holes or cavities[5-11] and arbitrary, geometrically based void linking criteria.[12-14]. The present study is based on modeling three-dimensional arrays of pores or voids by a two-dimensional random distribution of circular, through-thickness holes. The distribution of holes or "hole microstructure" may be characterized by three parameters: (a) the area fraction, (b) the hole size, and (c) the minimum interhole spacing, which controls the spatial distribution of holes and hole clustering. A focus of the study is to examine the void/pore linking process by determining the failure sequence of tensile specimens containing arrays of holes. An important

feature of this program is the strong interaction between experimental studies and computer simulation.

The experimental studies indicated a strong correlation between minimum interhole spacing and the mechanical properties of tensile specimens containing hole microstructures. Both the strength and ductility of the specimens were found to increase as the minimum interhole spacing increased or the degree of clustering decreased.[2-4] These studies also indicate that the specimens exhibit a dramatic decrease in ductility on changing from regular to random arrays of holes; this is indicated in Figure 1, which also illustrates the strong effects of the minimum interhole spacing. Experimental studies also indicate that the strain hardening of a material is very important in the void/pore linking process. This makes any prediction of void linking based on an arbitrary, geometric linking criteria[12-14] quite inadequate. For example, a void/pore looking criterion which provides a reasonable fracture strain for one material with a given void/pore distribution will very likely be incorrect for another material with differing strain hardening behavior or void/pore distribution.

The observed effects of the experimental studies can be readily understood through the use of a proposed physical model.[2,3] In the model, the fracture mechanism is a consequence of a four-step process:

First, local strain gradients develop near individual pores at small microscopic strains;

Second, upon further straining, failure of the ligament between closely spaced pores occurs due to flow localization. An elongated cavity is created by the ligament failure. Due to its eccentric shape, this cavity further localizes flow along its major axis;

Third, successive linking of adjacent pores occurs in a manner which is controlled by the spatial distribution of pores adjacent to those which have linked. Pore clustering is especially important in this stage as repeated linking results in increased strain concentration;

Fourth, the final stage of pore linking is triggered when a sufficient number of pores have linked to create an imperfection initiated macroscopic flow instability or crack-like defect. Again pore clustering is important as the generation of large local strains occur and percolation of the linking by a "void sheet" mechanism can occur.

This step-wise process of void linking lends itself to simulation by a computer model. As in three-dimensional void/pore linking, the computer model also relies on two input parameters: a

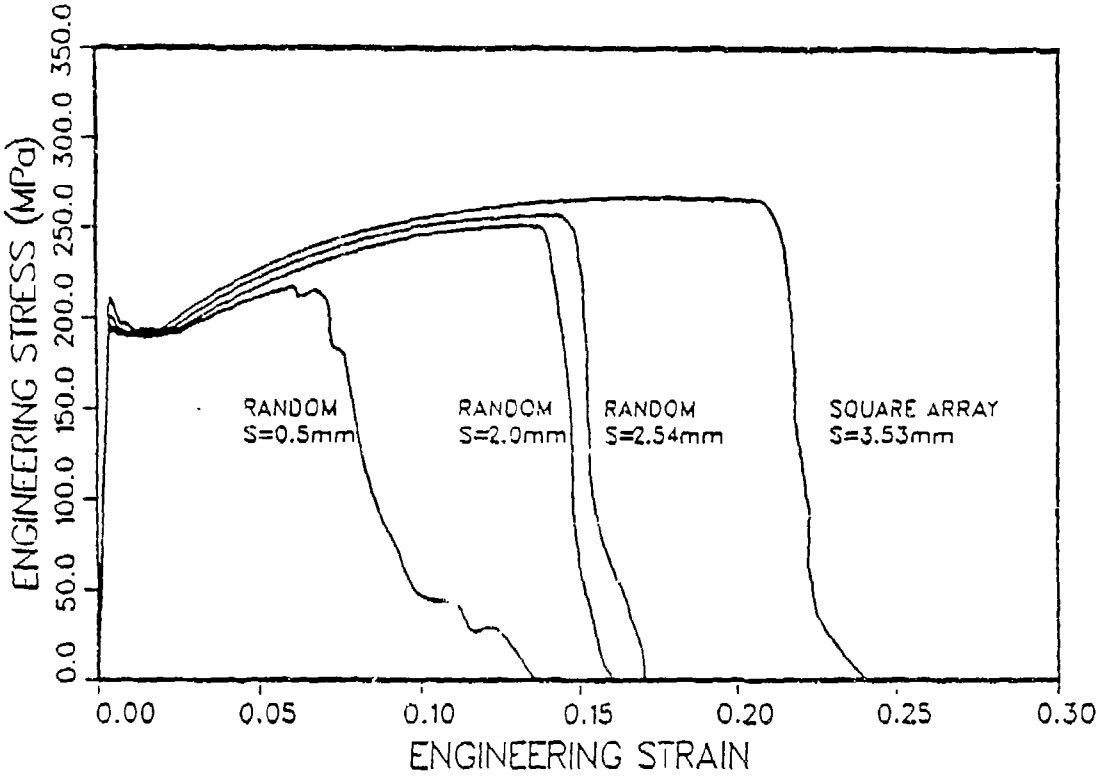

Figure 1. Engineering stress-strain behavior as a function of the minimum interhole spacing, (s), and the type of hole array for low carbon steel sheet. Data of Magnusen et al.[3]

description of strain localization near holes and a hole-linking criterion. In order to describe local strains near holes, experimental measurements of strain distributions near isolated holes, pairs of unlinked holes and linked holes were performed on 1100 aluminum and 70-30 brass sheet. These data were fit to equations which were then used to describe the strain localization of the above conditions in terms of hole parameters, material properties, and the applied strain. The computer model also relies on a critical thickness strain criterion for the failure of the ligament between adjacent holes.[15] It is important to note that the simulation uses no adjustable parameters other than those which experimentally describe the plasticity near the holes and the failure criterion for hole linking.

Figure 2 is an example of the agreement between the computer simulation and the experimental results for 1100 aluminum. For each point in the simulation, a minimum of ten computer runs were averaged in order to obtain statistically reliable predictions. In view of the absence of adjustable parameters in the computer simulation, the agreement between the predictions of the simulation and the experimental data is reasonable. Similar agreement is obtained for the higher strain-hardening, 70-30 brass.

In light of the reasonable agreement between prediction and experimental results, the computer simulation has recently been used to investigate (a) the effects of the specimen shape on ductile fracture[16] and (b) the effect of hole shape on ductility.[17] The specimen-shape study examined three specimen shapes all having identical gauge section areas but with length-to-width ratios which varied from 1:1 to 20:1. The simulation results indicated that specimen shape has several effects on the fracture of metals with large-scale porosity. First, ductility depends on specimen shape but only at small area fractures of porosity. In general, ductility decreases as the specimen's length-to-width ratio is increased; thus, short, wide specimens are expected to have greater ductility than their long, narrow counterparts at the same conditions of porosity. Furthermore, the effect is likely to be significant only at (1) small volume fractions of porosity, (2) when pores are clustered, and (3) when pores are large enough so that even a small cluster will create a significant reduction ($\sim 10^{-3}$) in lead-bearing area. Under these conditions, there will also

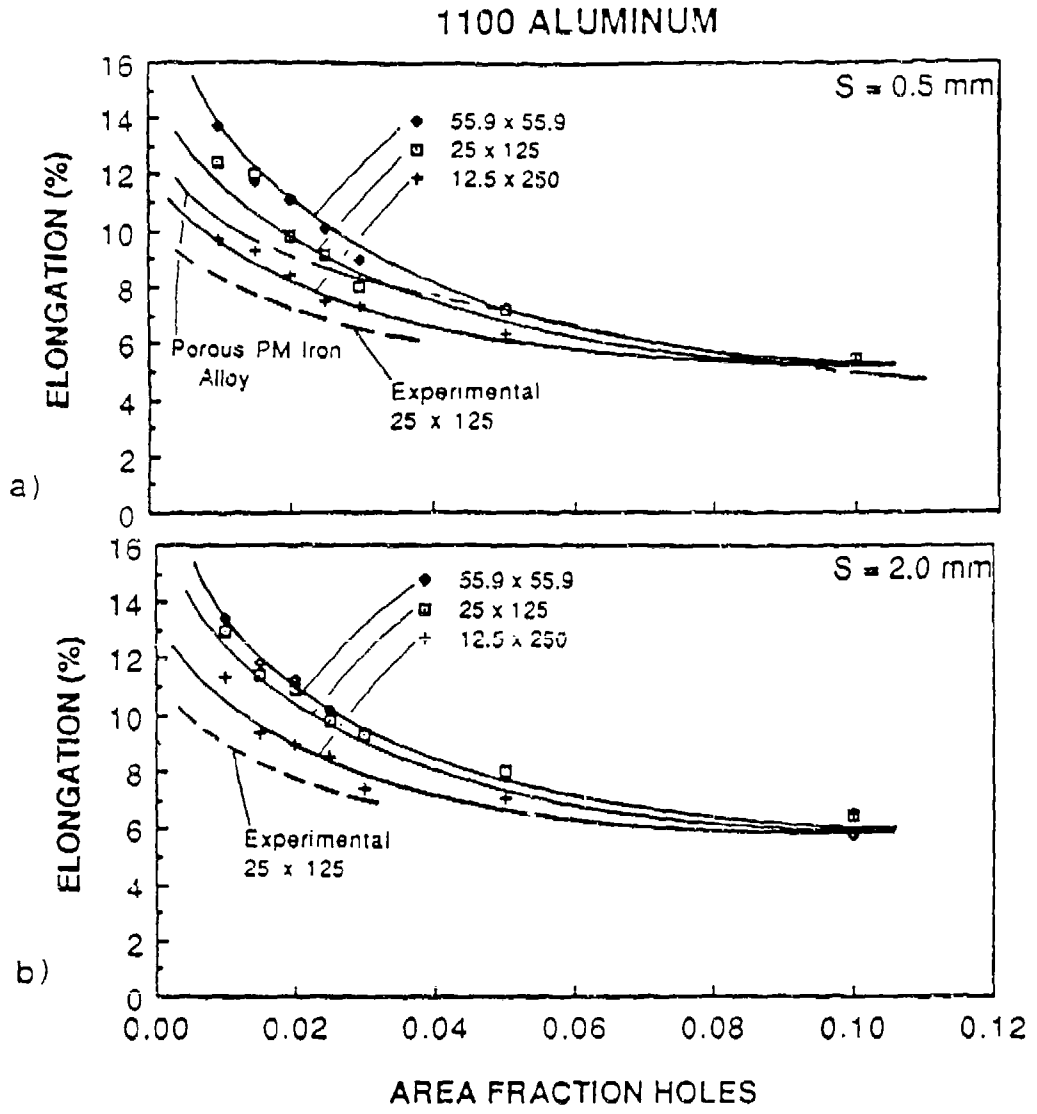

Figure 2 The dependence of the elongation to failure on the area fraction holes for 1100 aluminum. The diameter of the holes is 2.0 mm and the minimum allowable hole spacing are (a) 0.5 mm and (b) 2.0 mm. Data from the computer simulation are shown for specimen sizes of 55.9x55.9, 25x125 and 250 mms. The curves from the experimental model shown are from ref. [13,14] and in (a) the curve for porous PM iron is from ref. [30].

be a comparatively large scatter in ductility values from specimen to specimen. The analysis also predicts that the specimen shape effects will be most severe in materials with low strain hardening and minimal strain-rate hardening. These effects can be readily understood in terms of imperfection theory, which also provides a basis for understanding the fact that porosity usually influences tensile ductility much more than fracture toughness.[16]

The computer model was also extended in an initial attempt to examine the effect of void/pore shape on ductile fracture.[17] Two hole geometries were used in the simulations: an elongated hole which has a length to width ratio of 4/1 and a circular hole. The major axes of the elongated holes were maintained perpendicular to the tensile direction, since the strain localization effect of the elongated holes is maximized under this condition. The dimensions of the circular and elongated holes were selected such that the areas of the holes were the same. In the computer simulation, the strain fields of the elongated holes were obtained from empirical relations based on experiments utilizing pairs of circular holes in either 1100 Al or alpha brass which have been linked by a free surface prior to deformation. The specimens containing arrays of holes were simulated to deform under plane-stress conditions and to contain inhibited random arrays of through-thickness holes with area fractions which range from 0.01 to 0.10. Both specimen size and shape were kept constant since these can have significant effects on the ductility behavior of the specimens.[16]

The effect of hole shape on the ductility indicates the following trends:

1) The ductility of the specimens decreases as the area fraction of hole increases for both circular and elongated holes. This result is in accordance to previous work on the ductile fracture of porous materials, see ref. 1, for example.

2) The predicted ductility of the 'brass' specimens is greater than that of the '1100 Al.' This is consistent with increased ductility being associated with metals of high strain-hardening capacity.

3) As expected, the ductility of the specimens depends on hole shape in that the ductility of specimens with elongated holes is less than the ductility of specimens with circular holes. This is consistent with the ductility behavior of PM iron containing rounded vs. angular porosity.[18]

However, the present study indicates that the hole-shape effect depends on the area fraction of holes. Specifically, at low area fractions of holes such as 0.01 to 0.02, the hole-shape effect is small, while at high area fractions of holes (~0.01) the decrease in ductility due to the elongated hole shape is large. This effect occurs in both the 'Al' and the 'brass' specimens.

In summary, the computer simulation predicts a decrease in ductility due to presence of elongated holes or angular pores. However, the loss of ductility effect depends on the area fraction of holes and is most pronounced at large area fractions. These results can be understood in terms of a strain-induced hole/pore linking process. Under plane-stress conditions, the ligaments between neighboring holes fail at a critical thickness strain.[15] The effect of the hole (or pore) shape is to change the concentration of strain in the vicinity of the hole at a given macroscopic, applied strain. The magnitude of the strain-concentration depends on (1) the distance from the hole, (2) the shape of the hole, (3) the applied macroscopic strain level, (4) the strain hardening of the matrix, and (5) the location of neighboring hole. In particular, the elongated holes act to increase dramatically the level of local strain near a hole. Thus, the critical strain (or strain energy density) to initiate a crack or cause ligament failure is achieved at a smaller macroscopic strain if the holes are elongated. This results in accelerated hole linking and decreased ductility.

The prediction that the hole-shape effect depends on the area fraction of holes, being largest at high area fractions of holes, is quite reasonable in view if pore linking occurs by a localized flow instability process and not pore-induced crack initiation. The analysis of strains near holes indicates that distances greater than ~1 hole radius, the local strains are nearly equal for both circular and elongated holes. Thus, for large interhole spacings, the element of ligament material midway between holes cannot recognize whether the holes are elongated or circular. If hole linking occurs by a shear instability of the ligament when the "midway" element achieves a critical strain, then there will be very little accelerated hole linking due to elongated holes at large interhole spacings. This is the case at small area fractions of holes. Thus overlap of the intense parts of the local strain fields is much more likely to occur at large area fractions of holes or pores. As a result,

pore-shape effects are expected to be more pronounced at large area fractions of pores, provided that pore linking occurs by a flow localization process.

In summary, the present study has utilized a computer model which simulated three-dimensional pore distributions by two-dimensional arrays of through-thickness equalized holes in sheet specimens wherein deformation occurs primarily under plane-stress conditions. A principal advantage of the modeling approach is the ability to simulate the random nature of the spatial distributions(s) of pores or voids. The simulation is clearly a very simplified version of the realistic case in which pores of various shapes and sizes exist in three-dimensional space. However, difficulties in determining three-dimensional strain distributions and void/pore-linking criteria among random distributions of pores preclude a rigorous three-dimensional simulation at this time. Nevertheless, the methodology and the significant trends predicted by the present two-dimensional analysis establish the basis for understanding the strain-induced void/pore linking process in three dimensions and should serve as a basis for computational modeling of microvoid ductile fracture of structural alloys.

2. The Influence of Porosity on the Low Cycle Fatigue of Metals
(with Dale Gerard, Ph.D., November, 1988)

The in-service performance of powder-processed as well as cast materials is frequently limited by the presence of processing defects, notably porosity. Numerous investigations have examined the deleterious effects of porosity on high cycle fatigue and uniaxial tension behavior; see for example refs.1, 19-22. The reductions in high cycle fatigue life or porous specimens have been attributed to local stress concentrations near pores which result in localized slip even though the nominal stress remains elastic. Although there have been many studies investigating the effects of porosity on high cycle fatigue behavior of metals, there have been no fundamental studies examining the effects of porosity on low cycle fatigue behavior. This is significant since the resistance of metals to low cycle fatigue failure, wherein the materials is fully plastic, is often quite different than the response to high cycle fatigue when the nominal applied stress is elastic.

The purpose of this investigation was to examine in a detailed manner the influence of rounded porosity on low cycle fatigue behavior. Powder-processed titanium containing up to 6% rounded porosity (both isolated and continuous pores) has been used as a model system. Although this study is based on powder-processed materials, the results should also apply to cast materials which frequently contain residual porosity, or to those alloy/composite systems which readily form voids at small strains due to poor interfacial bonding or fiber fracture.

The influence of porosity on low cycle fatigue LCF has been studies using powder-processed titanium specimens tested at total strain amplitudes of 0.75 and 15% at 25°C. From a macroscopic standpoint, the following trends are most significant:

a. Porosity significantly influences the cyclic stress-strain behavior. For example, when compared to the cyclic flow response of fully dense titanium, even low levels of porosity (0.4%) cause the materials to behave cyclically as if it were being subjected to significantly higher strain amplitudes. This is interpreted to result from an enhanced level of localized plasticity which develops near the pores.

b. The low cycle fatigue life deteriorated rapidly with increasing volume fraction of porosity, strain amplitude, and especially when the porosity becomes interconnected. Even small amounts of porosity have a significant effect on LCF. For example, the presence of just 0.4% porosity decrease the LCF life by more than a factor of three at 1.5% total strain amplitude.

In order to evaluate mechanism of low cycle fatigue in the presence of pores, the influence of porosity on the individual stages of the fatigue failure process were thoroughly examined. In the investigation, fatigue failure was described by a four stage process consisting of the number of cycles for (1) a 15 μm microcrack to initiate, (2) microcrack(s) (i.e. short cracks) to grow and (3) link into a macrocrack, and (4) the macrocrack to propagate to failure. If any of the failure stages are accelerated by the presence of pores, a reduction in the low cycle fatigue life is eminent.

Pore-induced acceleration is especially large for microcrack initiation.[23] The acceleration of microcrack initiation appears to be essentially independent of the porosity levels and strain

amplitudes examined, but it is sensitive to the interconnectivity of the porosity. Specifically, 6% interconnected porosity accelerates crack initiation by a factor of about 100, compared to a factor of 10 for isolated porosity. Thus, while microcracks initiate in 800 cycles in the fully dense titanium at 1.5% total strain amplitude, only 9 cycles are required to initiate a similar crack at 6% interconnected porosity! Both the microcrack growth/linking and the macrocrack growth stages, also accelerate with increasing porosity level, strain amplitude and degree of interconnectivity of the porosity. In the case of microcrack growth and linking, the acceleration is more pronounced at large porosity levels, and especially for the case of interconnected porosity.

With regard to microcrack initiation, the following experimental observations/conclusions are pertinent:

(a) the enhancement of microcrack initiation due to porosity results in significant reductions in low cycle fatigue life,
(b) microcracks always initiate at pores,
(c) for the isolated-porous materials, the enhancement of microcrack initiation is essentially independent of the porosity levels at the strain amplitude examined, and
(d) when the porosity is interconnected, the microcrack initiation process is further enhanced as a result of the pores having a higher aspect ratio than the isolated porous materials.

An analysis of pore-induced microcrack initiation was successfully performed on the following basis[23]:

(a) The formation of the plastic zones near pores on the free surface of a plastically deforming matrix have been experimentally and theoretically modeled utilizing a through-thickness hole is metals deforming under plan stress conditions. A significant observation is that the strain profiles obtained adjacent to a hole indicate that no local strain accumulation occurs during LCF until approximately 80% of the fatigue life local to the hole.

(b) Using a Mason-Coffin relationship[24,25] as a local failure criterion in conjunction with a cumulative damage law, the number of cycles to initiate a 15 μm crack was predicted from estimates of the maximum strain amplitudes near pores, as determined by the modified Neuber analysis.[26] The predictions of this analysis were in excellent agreement with the experimental data over a range of pore contents and at both strain amplitudes. It should be noted that this is a general analysis and applies to LCF crack initiation in any metal containing porosity of arbitrary shapes which can be described by stress concentration factors; only the cyclic stress-strain response of the matrix needs to be known.

With regard to the growth of short cracks, in the presence of porosity, the following characteristics are most significant:[27]

(a) Isolated rounded porosity temporarily accelerates short fatigue crack growth rates as a result of large plastic strains within the plastic zones of the pores. Outside of the plastic zones,

which scale with the pore size, short cracks propagate at rates which are similar to those which are expected in a fully dense materials.

(b) Crack closure of short cracks has been observed to occur at the crack-tip only at highly compressive loads. Portions of the crack behind the tip appeared to remain open during the entire cycle. The short crack-tips open early in the tensile loading portion of the cycle, "peeling" open from the center toward the tip of the crack. It appears that porosity does not influence short crack closure during high-strain fatigue testing.

The role of porosity in microcrack linking during the LCF of porous materials may be understood as follows:

(a) The microcrack linking process is accelerated by porosity as a result of a higher density of microcracks.

(b) When comparing the acceleration of the microcrack linking process directly among the different porosity levels, only minimal increases in the linking rate which observed when the isolated-porosity level is increased from 0.4% to 6%. This is attributed to a saturation density of microcracks which is very similar over this porosity range.

(c) The influence of porosity on microcrack linking is significantly less at the 0.75% total strain amplitude. This appears to be a result of a much lower density of microcracks being initiated throughout the fatigue life for all the conditions which have been examined.

(d) Because of the interaction between short crack growth and microcrack linking, a rigorous theoretical analysis of the number of cycles to grow and link microcracks into a macrocrack could not be performed. However, a semi-qualitative analysis based on crack length distribution at the onset on lone crack growth could be used to estimate the number of cycles from crack unification to the onset of long crack growth.

Macrocrack propagation is affected by porosity in the following manner:

(a) Porosity accelerates the overall macrocrack growth rates, as approximated by the number of cycles for a macrocrack to propagate through the specimen, by factors of roughly tow to four.

(b) The closure stress for macrocracks is not significantly influenced by the presence porosity during high-strain fatigue.

(c) By incorporating a lineal roughness parameter, porosity-induced increases in the macrocrack growth rates are quite large for the 6% porous materials when the actual distances over which the crack propagates are considered. At the lower porosity levels the macrocrack growth rates are only nominally larger when the lineal roughness parameter is taken into consideration.

(d) A qualitative model was developed which physically accounts for the accelerated growth rates of macrocracks in the porous materials. The model assumes minimal differences in crack closure behavior between the porous materials. The model assumes minimal differences in crack closure behavior between the porous and fully dense materials, as is observed experimentally. The model is based on the concept that the acceleration of macrocrack growth in the presence of porosity at large strain amplitudes is a result of the interaction of the crack-tip plastic zone with the pore-induced plastic zones resulting in shear instabilities. These shear instabilities contribute to an additional crack growth component.

In summary, the present study has provided a detailed, systematic insight into the mechanisms by which porosity affects low cycle fatigue. Both experiment and modeling approaches were used with modeling being especially effective in predicting the influence of porosity on fatigue crack initiation.

3. Deformation of Rapidly Solidified Dispersion-Strengthened Titanium Alloys (with Stephen L. Kampe, Ph.D.)

OXIDE DISPERSING STRENGTHENING (ODS) of titanium-based alloys creates the potential of a new generation of lightweight, high-performance alloys with improved strengths and creep properties at elevated temperatures. The improvements in mechanical performance have been attributed to the presence of insoluble oxide particles which act as barriers to dislocation motion and remain microstructurally stable even to high temperatures. A principal difficulty encountered in the development of ODS alloys is the need for a processing technique capable of creating a uniform distribution of finally spaced, insoluble particles. However, the recent application of rapid solidification (RS) techniques to titanium -based alloys have indicated the potential to obtain oxide particle dispersoids distribution homogeneously within the matrix. These alloys utilize rare earth elemental additions to titanium because of their ability to scavenge interstitial oxygen from titanium solid solution and form a dispersion of thermally stable rare earth oxide precipitates.

Previous research established the potential of RS in oxide dispersion-strengthened titanium alloy development through extensive evaluation of the thermal stability of candidate microstructures in the unconsolidated form of ribbon, flake, or splats (see, for example REF 28-38). However, none of these studies were aimed at establishing the controlling deformation mechanisms in fully processed bulk material. This research program examined the strength and high temperature flow behavior over a much wider range of temperatures, strain-rates, and stresses than previously examined[39,40]. It focused on a range of alloy compositions based on the technologically important Ti-Al system alloyed with elemental erbium. Particular attention was given to analyses of mechanisms of plastic flow at elevated temperatures, as well as the influence of microstructure, especially matrix grain size, dispersoid size and distribution, on the observed behavior. A summary of the principal results follows below.

When consolidated into bulk form, Ti-Er and Ti-Al-Er alloys produced by rapid solidification techniques retain a fine and homogeneous dispersion of oxide particles with fine-grain (3-5 μm) matrices. In the as-consolidated form, the majority of the dispersoids are very fine (average

diameter ~40-80 nm) and generally reside within the interiors of the matrix grains. A few large dispersoids (diameter >200 nm) are also present; most of these are located on grain boundaries. Both the dispersoids and fine grains microstructure present in the as-processed alloys are extremely resistant to coarsening during high temperature anneals at temperatures near the beta-phase transus temperatures. An order-of-magnitude increase in grain size is achieved only by heat treatments at temperatures within the beta-phase field; however, this is accompanied by significant dispersoid coarsening and in some cases additional dispersoid formation.

Results from compression testing of the Ti, Ti-Er and Ti-Al-Er alloys over a range of temperatures (20° to 755°C) and strain rates ($5x10^{-5}$ to 6×10^{-3} s^{-1}) indicate that the yield and flow strength of these alloys are sensitive to temperature, strain rate, grain size and alloy composition. For example, at room temperature the addition of erbium results in lower yield strengths; this is believed to be caused by a reduced solid solution strengthening component due to oxygen depletion as a result of the internal oxidation of the erbium to erbia. As the temperature is increased, oxygen loses its effectiveness at a strengthener; strength of these alloys at higher temperatures rely on contributions from aluminum in solid solution and particle strengthening from the stable oxide dispersoids.

Based on the conditions imposed in the present study, the high temperature deformation of these dispersion-strengthened titanium alloys is characterized by a "two stage" deformation behavior, which strongly suggests that two distinct deformation mechanisms are operative over the specific ranges of temperature, strain rates, and stresses. In the range of high temperatures and low stress/strain rates ($\dot{\varepsilon}/D \leq 1 \times 10^{12}$ m^{-2}), the mechanical test data and post-deformation microscopy indicate that grain boundary sliding is the rate-controlling deformation mechanism in the fine grain alloys. Increasing the grain size from 3-4 μm to 25-40 μm enhances the high temperature strength and creep resistance of the strengthened titanium alloys. This occurs as a result of (a) a minimization or elimination of grain boundary sliding as the dominant deformation mechanism due tot the reduction of grain boundary area, (b) an increased density and size of dispersoids residing on grain boundaries, also acting to minimize grain boundary sliding by

mechanically "pinning" the boundaries, and (c) additional precipitation of oxide particles which occur during the high temperature grain growth anneals, thus providing additional particle strengthening. The experimental behavior are in good agreement with constitutive equations which model deformation via grain boundary sliding mechanisms.

For low temperatures/high strain rates conditions the mechanical test date are consistent with a deformation mechanisms of dislocation creep past obstacles. Post-deformation microscopy reveals evidence of significant dislocation-dispersoid interaction in alloys tested under these conditions of temperature and strain rate ($\dot{\bar{\varepsilon}}/D \geq 10^{12}\ m^{-2}$). The apparent grain size effect in the dispersoid-containing alloys under these conditions is interpreted to be a result of an increased population of dispersoids which evolve during the high temperature grain-growth anneals.

4. On the Influence of Strain-Path Changes on Fracture (with Susan Kestner, M.S.)

The effect of strain-path changes on microvoid ductile fracture has not been examined in detail. Studies based on proportional loading clearly show that the fracture strain for a ductile, microvoid fracture process is a function of both stress state and strain-path (for example, see ref's. 41-43). Thus, it would be reasonable to expect that ductile fracture should be a function of strain-path history. The purpose of this study was to present unique data which indicate that ductile fracture, at least in certain cases, is strongly dependent on changes in strain-paths imposed prior to failure.[44]

As show in Fig.3, data indicate that ductile, microvoid fracture does indeed depend on nonproportional strain-path history. In particular, a combination of uniaxial and equibiaxial tension can result in a significant ductility enhancement at a final strain state of plane-strain tension. The ductility enhancement occurs for Ti either with or without void-nucleating hydrides. The effect is most pronounced for material without hydrides when subjected to a sequence of equibiaxial prestrain followed by uniaxial strain path to failure. Although we expect the total fracture strain to depend to strain path, we do not have complete explanation for the above effects.

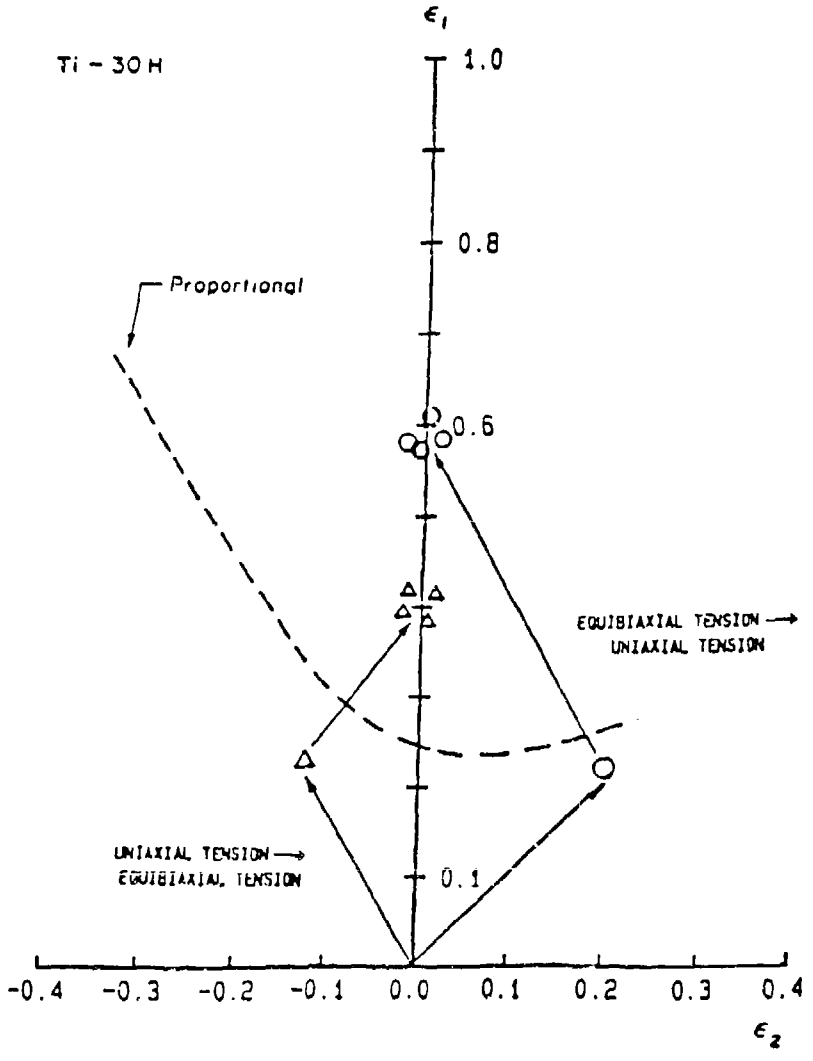

Fig. 3 The influence of strain path on the major and minor principal strains at fracture of titanium sheet containing 30 wt ppm H.

One contributing factor may be a delay of void nucleation during multi-stage straining by using strain paths characterized by small maximum principal stresses.

5. Microstructure and Properties of a Powder-Processed, Rapidly Solidified (Cu-Nb)-Mo alloy. (with Kevin Zeik, Ph.D. candidate)

The presence of sharp, cyclic thermal transients in structural components operating at high temperatures, sometimes in the presence of hydrogen, require not only high temperature strength, thermal stability and resistance to environment embrittlement but also a high degree of thermal conductivity. Existing alloys for such applications, typically copper-and aluminum-based alloys, suffer from various problems, from poor ductility to a lack of high temperature (>600°C) thermal stability. Thus, in order to meet the desired design criteria, new alloys must be developed.

Recently, extensive wire drawing of Cu-based alloys containing insoluble, ductile second-phases has let to significant advances in the strength of high conductivity materials. The deformation-processed Cu-Nb alloys, however, suffer from severe morphological instabilities when exposed to temperatures exceeding 350°C [45]. Previous research has shown that the high strengths achieved be deforming the niobium second-phase into ultra-thin (50 Å) ribbons is lost when the alloy is exposed to 350°C for 24 hours; the ribbons coarsen to twice their original thickness [45]. The high surface energy associated with the ribbon morphology, in addition to rapid diffusion along the interfaces, was determined to be responsible for the thermal degradation of ribbon morphologies [46]. Therefore, these composites have limited high temperature service capabilities.

The purpose of this research is to examine the strength and thermal stability behavior of a Cu-Nb base alloy processed by non-conventional solidification processing, specifically high pressure gas atomization (HPGA). The result is a material characterized by unique equiaxed microstructures consisting of a high volume fraction of thermally stable multiphase spheroids and Nb-rich dendrites distributed within a continuous copper matrix.

High pressure gas atomization (HPGA) has been used to produce rapidly solidified Cu-21 Nb-1.8Mo (wt%) alloy powders with a range of microstructures found to be dependent on powder

size. Specifically as shown in Fig.4, the microstructures of fine-scale powders (<15μm dia.) were characterized by a predominance of multiphase spheroids and a small population of Nb-based dendrites distributed within an almost pure copper matrix. In contrast, the larger particles (>45μm dia.) were found to contain only Nb-based dendrites distributed within a copper matrix. Due to the multiphase spheroids, the volume fraction of "second-phase" is much higher in the former instance, 35%, than in the latter, 22%.

The change in microstructure as a function of powder particles size has been analyzed in term of both the amount of undercooling and the cooling rate of the liquid droplets prior to and during initial solidification.[47] In particular, the large amounts of undercooling attained by the fine droplets are believed to induce a non-equilibrium liquid-phase separation which results in the formation of spheroidal, multiphase Nb-Cu-Mo particles within a copper rich matrix. As expected, the secondary dendrite arm spacing as well as the size of the spheroids decreased with increasing cooling rate (decreasing particle size).

The yield behavior of material produced from the HPGA powders was found to be controlled by a combination of grain-size (Hall-Petch), particle-hardening (Orowan) and dislocation-substructure strengthening. The difference in room temperature yield strength between material produced from fine (<10μm dia.) powders, 460 MPa, and coarse (45-63 μm dia.) powders, 300 MPa, was interpreted to result primarily from a significant difference in the interparticle spacings, which affects the Orowan strengthening contribution. At 600°C, the effects of recovery processes, presumable due to cross-slip and thermally activated dislocation climb, render short-range obstacles relatively ineffective. This causes a decrease in the yield strengths of the HPGA materials as well as pure copper.

The flow behavior of the Cu-21.2Nb-1.8Mo (wt%) HPGA alloys was characterized by parabolic-type hardening at small strains (<0.20) followed either by linear hardening (Stage IV) or zero-hardening (flow stress saturation), depending on test temperature. A typical example is shown in Fig.5, in which the regime of parabolic strain-hardening at small strains was analyzed in terms of the geometrically necessary dislocations and associated interactions which occurred as a

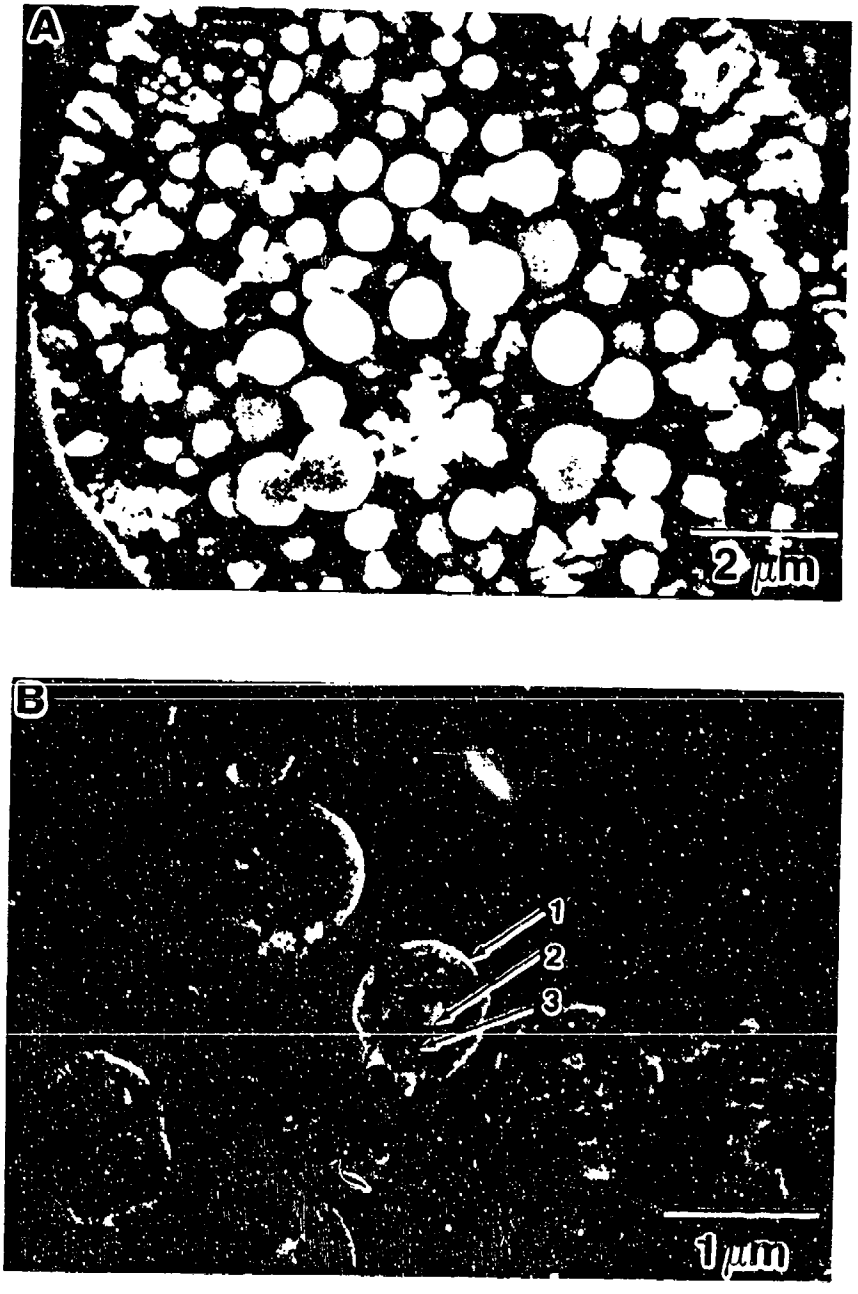

Figure 4 Scanning electron micrograph of a) the microstructure of a single, small (10μm dia.) powder particle and b) a cross-section view of one single composite spheroid contained within this microstructure.

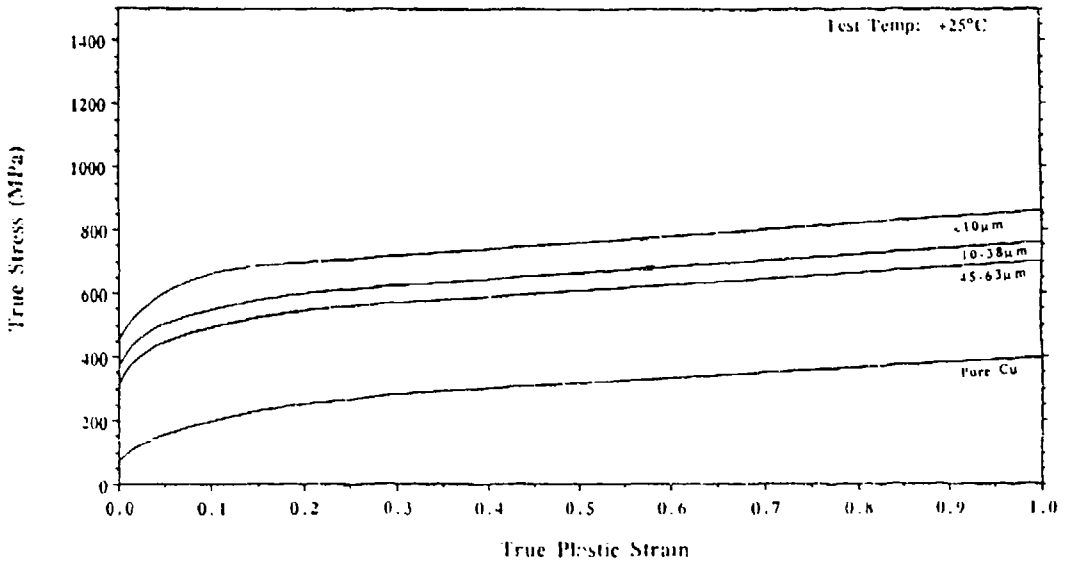

Figure 5 True stress - true strain behavior of Cu-21Nb-2Mo specimens processed from HPGA powders of the indicated size ranges.

result of the strain-incompatibility between the matrix and the Nb-rich second-phase dispersions. As deformation continues, recovery processes increasingly influence the flow behavior. At large strains and at T<600°C, a transition to linear-hardening (Stage IV) occurs; this may be due to incomplete annihilation of screw dislocation segments during cross-slip (i.e. incomplete recovery). At 600°C the increased rate of recovery processes result in balance between strain-hardening and recovery events, causing the flow stress to saturate with further deformation (zero-hardening). At large strains, Stage IV hardening was found to be only a function of strain and temperature and not a function of microstructure.

Finally, the thermal stability of these materials was analyzed in terms of the resistance of the second-phase dispersions to coarsening during high-temperature (900°C, $0.83T_{mp}$) anneals. The greatly improved thermal stability of the HPGA microstructures as compared to that of the in-situ, deformation processed Cu-Nb alloys of similar composition is related to the morphology of the dispersed phase. Furthermore, due to the limited solubility and diffusively of copper in niobium, the composite nature of the multiphase spheroids is retrained after 100 hours at $0.83T_{mp}$; thus the enhanced volume fraction of "second-phase" is maintained within materials produced from fine (<10μm dia.) HPGA powders. This microstructural stability was demonstrated by both microhardness and stress/strain results. The hardness of materials exposed to 900°C for 1000 hours decreased by only 16-22% while the yield stress decreased by 20-29%. The larger decreases observed for material produced from the fine (<10μm dia.) powders is attributed to some Ostwald ripening of very fine (<50mn) multiphase spheroids. In all instances, the second-phase dispersion was quite effective at preventing grain growth during high temperature exposures.

6. A New Age-Hardenable Beta Titanium Alloy (with Lou Quattrocchi, M.S. Candidate).

The use of titanium alloys in aerospace and other industrial applications has steadily increased over the last 40 years. Most of these applications use alpha-beta titanium alloys which, because of their poor formability, are expensive to process. Furthermore, despite their excellent strength at relatively high service temperatures, alpha-beta alloys are also susceptibility to hydrogen

embrittlement. A particular class of titanium alloys that possesses good resistance to corrosion and hydrogen embrittlement as well as excellent formability is the beta titanium alloys. Beta titanium alloys exhibit good forming qualities in the solution-treated condition and can be age hardened to yield strengths of 1100-1200 MPa [48]. However, the use of existing beta alloys have been limited in part because they rely on the formation of alpha-phase precipitates of age hardening. As such, they do not possess the necessary microstructural stability at high temperature (T>400°C), and their elevated temperature strength or creep resistance is poor [48]. Thus, to fully exploit the properties of beta titanium alloys for high temperature applications, an alloy with improved microstructural stability at elevated temperatures is very desirable.

An unexplored alternative to the existing beta titanium alloys are alloys based on the intermetallic compound Ti_3Al as a hardening phase. In the last decade, titanium aluminides based on both Ti_3Al and TiAl have shown promise as a low density material with high temperature strength. A major problem with Ti_3Al (as well as TiAl) as a structural material is its poor room temperature ductility and fracture toughness. However, this problem would be alleviated if the Ti_3Al would be incorporated as discrete particles into a ductile, tough matrix, such as the bcc beta phase. Thus, the purpose of this study is to examine the age hardening behavior of a beta Ti alloy strengthened by the formation of ordered alpha-two precipitates.

The present study was undertaken to develop an understanding of the age-hardening behavior and the associated stress-strain responses of the Ti-23Nb-11Al alloy in terms of microstructural evolution. Results from this research have established the following:

1) Based on optical microscopy, the second-phase solvus of the alloy was determined to be 960 ±15°C. After quenching from solution-treatment temperatures, the alloy exhibited a large age-hardening response when it was aged between 375°C and 675°C. Peak age-hardening of the alloy occurred when it was aged at 575°C for 6 hours.

2) In the solution-treated (S/T) condition, TEM examination revealed the alloy was a single-phase with a disordered, bcc-type lattices. There was no indication of the presence of the ω-phase in the TEM examination of the S/T condition or any of the aged conditions. After

subsequent aging at 375°C for 100 hours, the microstructure retained the disordered bcc matrix but contained very small (5-10 nm) precipitates whose structure could not be identified with certainty. In the S/T and aged at 575°C for 6 hours condition, the alloy microstructure contained lath-like precipitates identified at α_2-phase, whose average dimensions were: a-170 nm, b-120 nm and c-30 nm. Upon aging at 675°C for 100 hours, lath-like, alpha-two precipitates form with average dimensions of a=500 nm, b=170 nm and c=80 nm. In all of the aged conditions, the matrix remained disordered beta phase.

3) At low temperatures (-196°C to 25°C), the yield strength of the alloy exhibited a rapid increase with decreasing temperature. This was attributed to thermally activated dislocation motion past obstacles such as interstitial oxygen, substitutional solid-solution Al and Nb, and a significant Peierls force. For intermediate temperatures (25°C to 527°C), the yield strength of the alloy was relatively independent of temperature.

4) The compression stress-strain response at temperatures between -196°C and 327°C, indicated that, in all heat-treated conditions the alloy exhibited rapid strain-hardening for strains less than about 0.04. At strain exceeding 0.04, linear strain-hardening ($d\sigma/d\varepsilon$ = constant) was observed for all of the heat-treated conditions.

5) Deformation at room temperature occurred by the formation of intense, non-uniform slip bands for all heat-treated conditions, except after aging at 675°C. The presence of the coarse slip was attributed to repeated shearing of precipitates, which concentrated slip on particular slip planes. Upon aging at 675°C, there were no observable slip lines; this was likely are result of dislocations looping around precipitates, which causes a very fine, homogeneous distribution of slip.

6) Serrated yielding was observed during testing of the alloy in the S/T condition and condition at a test temperature of 327°C. The occurrence of serrated yielding was attributed to dynamic strain aging (DSA). The evidence linking DSA to serrated yielding was the presence of a negative strain-rate hardening exponent as well as an increase in strain-hardening. As estimated from diffusion calculations, interstitial oxygen was likely the cause of the DSA process.

7) The strain-rate hardening exponent of the alloy was very small or negative at intermediate temperatures. The negative m-value for the S/T condition and the S/T and aged at 375°C condition was attributed to dynamic strain aging.

8) All specimens failed in a ductile manner during room temperature tensile tests. In the S/T condition, the alloy was very ductile, as evidenced by the macroscopic deformation along the gauge length and the large dimples present on the fracture surface. When the alloy was aged at 375°C and 575°C, the ductility was very limited. The low ductility was attributed to dislocations shearing precipitates, which lead to intense slip bands and associated stress concentrations. As a result, the fracture occurred via decohesion of coarse, planar slip bands, resulting in a transgranular fracture path. After aging at 675°C, the alloy showed improved ductility as a result of a homogeneous distribution of slip when dislocations looped around precipitates. The fracture path in this condition was both transgranular and intergranular; the intergranular fracture path was attributed to the presence of grain boundary precipitates, as evidenced by the intergranular fracture surface,which contained dimples on the order of the precipitate size (200nm).

REFERENCES

1. R. Haynes, The Mechanical Behavior of Sintered Alloys, (Freund Publishing House, London) 1981.
2. E. M. Dubensky and D. A. Koss, Metall, Trans A. 184, P. 1887 (1987).
3. P. E. Magnusen, E. M. Dubensky and D. A. Koss, Acta Metall. 36, p. 1503 (1988)
4. P. E. Magnusen, D. J. Srolovitz and D. A. Koss, Acta Metall. 38, 205 (1990).
5. F. A McClintock, J. of Appl. Mech., 35, p. 363 (1968).
6. A Needleman, J. of Appl. Mech., 39, p. 964 (1962).
7. M. Nagumo, Act Metall., Mech., 21, p. 1661 (1973).
8. B. I. Elelson, Trans. ASM, 56, p. 82 (1963).
9. P. F. Thomason, Acta Metall., 29, p. 763 (1981).
10. V. Tvergaard, Int. J. Frac., 17, p. 389 (1987) and 18, p. 237 (1982).
11. P. F. Thomason, Acta Metall., 33, pp. 1079 and 1087 (1985).
12. L. M. Brown and J. D. Embury, in Proc. 3rd Int. Conf. Strength of Metals and Alloys, p. 164 (1973).
13. R. A. Tait and D. M. R. Taplin, Scripta Met., 13, p. 77 (1979).
14. G. LeRoy, J. D. Embury, G. Edward and M. F. Ashby, Acta Metall., 29, p. 1509 (1981).
15. P. L. Magnusen and D. A. Koss in Developments in Mechanies 15, 421 (1991).
16. A. Geltmacher and D. A. Koss, Int. J. Powder Metall., 26, 205 (1990).
17. A. Geltmacher and D. A. Koss in 1990 Adv. in Powder Metall., 3, 37 (1990).
18. K. M. Vedula and W. M. Heckel, Modern Developments in PowderMetallurgy, Vol. 12 eds. H. H. Hausner, H. W. Antes and D. D. Smith, MPIF, 1981.
19. M. Eudier, Powder Metall., 9, pp. 278-290 (1962).
20. R. Haynes, Powder Metall., 1, pp. 17-20 (1977).
21. R. J. Boucier, D. A. Koss, R. E. Smelser and O. Richamond, Acta Metall., 34 (12), pp. 2443-2453 (1986).
22. P. R. Smith, D. Eylon, S. W. Schewnker and F. H. Froes, Advanced Processing Methods for Titanium, Eds. D. F. Haason and C. H. Hamilton (TMS-Varrendale), p. 61 (1981).
23. D. A. Gerard and D. A. Koss, Mat. Sci. and Eng. A129, 77 (1990).

24. S. S. Manson and M. H. Hirschberg, Fatigue: An Interdisciplinary Approach (Syracuse Univ. Press, Syracuse, NY) p. 133 (1964).

25. L. F. Coffin, Jr., Trans. ASM 561, p. 438 (1959).

26. H. Neuber, Trans. ASME, p. 544 (1961).

27. D. A. Gerard and D. A. Koss to be published inInt. J. Fatigue.

28. Processing of Structural Materials by Rapid Solidifaction (conf. proc.), ed. F. H. Froes and S. J. Savage, ASM, 1987).

29. F. H. Froes and R. G. Rowe: in Titanium Rapid Solidifaction Technology (proc. conf.), ed. F. H. Froes and D. Eylon, TMS-AIME, 1986, 1-19.

30. S. M. L. Sastry, P. J. Meschter, and J. E. O'Neal: Metall. Trans A, 1984, vol. 15A 1451-63.

31. D. B. Snow and A. F. Giamei: in Titanium Rapid Solidfication Processing (proc. conf.), ASM-AIME, 1986, 153-64.

32. S. H. Whang: J. Mater. Sci., 1986, volv. 21 (7), 2224-38.

33. S. M. L. Sastry, T. C. Stanley, M. H. Loretto, and H. L. Fraser: Acta Metall., 1986, vol. 34 (7), 1269-77.

34. D. G. Konitzer, J. T. Stanley, M. H. Loretto, and H. L. Fraser: Acta Metall., 1986, volv. 34 (7), 1269-77.

35. F. H. Froes and R. G. Rowe: in Rapidly Solidified Alloys and Their Mechanical and Magnetic Properties (proc. conf.), ed. B. C. Giessen, D. POlk, and A. I Taub, 1986, 209-334.

36. D. G. Konitzer and H. L. Fraser: in High Temperature ordered Intermetallic Alloys (proc. conf.), ed. C. C. Koch, C. T. Lius, and N. S. Stoloff, MRS, 1985, 437-42.

37. D. G. Konitzer, D. C. Muddle, and H. L. Fraser: Scripta Metall., 1983, vol. 17, 1983, 963-66.

38. R. G. Rowe, T. F. Broderick, E. R. Koch=h, and F. H. Froes: in Rapidle Solidified Materils (proc. conf.), ed P. W. Lee and R. S. Carbonara, 1985, 107-14.

39. S. L. Kampe and K. A. Koss: in Processign of Structural Metals by Rapid Solidification (proc. conf.), ed. F. H. Froes and S. J. Savage, ASM, 1987, 175-80.

40. S. L. Kampe and D. A. Koss, Metall. Trans. A 20A, 875 (1989).

41. S. L. Semiatin, J. H. Holbrook, and M. C. Mataya: Metall, Trans. A., 1985, vol. 16A, P. 145.

42. R. J. Bourcier and D. A. Koss: Acta Metall., 1984, volv 32, p. 2091.

43. G. LeRoy, J. D. Embury, G. Edward,a nd M. F. Ashby: Acta Metall., 1981, vol.29, p. 1509.

44. S. Kestner and D. A. Koss, Metall. Trans. A, 18A, 637 (1987).

45. J. D. Verhoeven, H. L. Downing, L. S. Chumbley, and E. D. Gibson, J. Appl. Phys., 65, (1989) p. 1293.

46. J. Malzahn-Kampe, Ph.D. Thesis, Mechigan Technological University, 1989.

47. K. Zeik and K. A. Koss, Tech. Rep. No. 17, ONR Contract N000 14-86-K-0381, July 1990.

48. Beta Titanium Alloys in the 1980's (TMS-AIME< Warrendale), 1984.

LIST OF PUBLICATIONS/REPORTS/PRESENTATIONS OF ORN CONTRACT N00014-86-K-0381 FOR THE PERIOD

5/36 - 11/90

Papers published in Referred Journals

1. "On the Influence of Strain-Path Changes of Fracture" (with S. Kestner), Metall. Trans. A. 18A, 637 (1987).

2. "The Influence of Porosity on the Deformation and Fracture of Alloys" (with R. J. Bourcier, R. D. Smelser, O. Richmond), Acta Met 34, 55 (1986).

3. "Void/Pore Distributions and Ductile Fracture" (with E. M. Dubensky) Metall. Trans. A, 18A, 1887 (1987).

4. "Densification of Titanium Powder During Hot Isostatic Pressing" (with B. K. Lograsso), Metall. Trans. A 19A, 1767 (1988).

5. "The Effect of Void Arrays on Void Linking During Ductile Fracture" (with P. E. Magnusen, E. M. Dubensky), Acta Metall. 36, 1503 (1988).

6. "Stress State and Hydrogen-Related Fracture" (with Fan Yunchang) Res Mechanical 24, 1 (1988).

7. "Deformation of Rapidly Solidified Dispersion Strengthened Titanium Alloys", (with S. L. Kampe) Metall. Trans. A 20A, 875 (1989).

8. "A Criterion for Hole/Void Linking Under Plane-Stress Conditions", (with P. L. Magnuson) in Developments in Mechanics 15, 421 (1989).

9. "Low Cycle Fatigue Crack Initiation: Modeling the Effect of Porosity" (with D. A. Gerard) Int. J. Powder Metall, 26, 337 (1990).

10. "A Simulation of Void Linking During Ductile Fracture" (with P. E. Magnusen and D. J. Srolovitz), Acta Metall. 38, 1013 (1990).

11. "A Computer Simulation of Specimen-Shape Effects and Ductility of Porous Metals" (with A. Geltmacher), Int. J. of Powder Metallurgy 26, 205 (1990).

12. "Porosity and Crack Initiation During Low Cycle Fatigue (with D. A. Gerard), Mat'l. Sci. and Eng. A 129, 77 (1990).

Papers Published in Symposia/Proceedings/Books

1. "Deformation of Rapidly Solidified Ti-2Er" (with S. L. Kampe in Enhanced Properties in Structural Metals via Rapid Solidification (ASM, Metals Park, OH), 1987.

2. "Microstructure and Mechanical Properties of a Powder-Processed Cu-Nb Alloy," (with K. Zeik, I. Anderson, and J. Vehoevan), Proc. to Powder Metallurgy Key to Advanced Materials, (ASM, Metals Park), 1990.

3. "On Modeling the Effect of Pore Shapes on Ductile Fracture" (with A. Geltmacher in 1990 Adv. in Powder Metall. 3, 37 (1990).

4. "Cyclic Stress-Strain Behavior of Titanium in the Presence of Porosity" (with D. A. Gerard) 1990 Adv. in Powder Metallurgy, 3, 37 (1990).

Technical Reports

1. "On the Influence of Strain-Path Changes on Fracture" (with S. Kestner), Technical Report No. 1, ONR Contract No. N00014-86-K-0381, August 1986.

2. "Stress State and Hydrogen-Related Fracture" (with F. Yunchang), Technical Report No. 2, ONR Contract No. N00014-86-K-0381, September 1986.

3. "Deformation of Rapidly Solidified Ti-2Er" (with S. L. Kampe), Tech. Report No. 3, ONR Contract No. N00014-86-K-0381, September 1986.

4. "Densification of Titanium Powder During Hot Isostatic Pressing" (with B. K. Lograsso), Technical Report No. 4, ONR Contract N00014-86-K-0381, January, 1987.

5. "Ductile Fracture and Random vs. Regular Hole/Void Arrays" (with P. E. Magnusen and E. M. Dubensky), Technical Report No. 5, ONR Contract N00014-86-K-0381, February, 1987.

6. "Advanced Processing and Properties of High Performance Alloys"Technical Report No. 6, ONR Contract N00014-86-K-0381, February, 1987.

7. " Simulation of Void Linking During Ductile Fracture" (with P. E. Magnusen and D. J. Srolovitz), Technical Report No. 7, ONR Contract N00014-86-K-0381, September, 1987.

8. "Deformation of Rapidly Solidified Dispersion Strengthened Titanium Alloys" (with S. L. Kampe), Technical Report No. 8, ONR Contract N00014-86-K-0381, December 1987.

9. "Advanced Processing and Properties of High Performance Alloys", Tech. Report No. 9, ONR Contract N00014-86-K-0381, March, 1981.

10. "The Influence of Porosity on Short Fatigue Crack Growth at Large Strain Amplitudes" (with D. A. Gerard), Tech. Report No. 10, ONR contract N00014-86-K-0381, July 1988.

11. "On Specimen Shape Effects and The Ductility of Porous Metals" (with A. Geltmacher), Technical Report No. 11, ONR Contract N00014-86-K-0391, February, 1989.

12. "Advanced Processing and Properties of High Performance Alloys", Tech. Report No. 12, ONR Contract N00014-86-K-0381, April, 1989.

13. "Porosity and Crack Initiation During Low Cycle Fatigue", (with D. Gerard) Technical Report No 13, ONR Contract N00014-86-0381, July, 1989.

14. "On Modeling the Effect of Pore Shapes on Ductile Fracture" (with A. Geltmacher) Technical Report No. 14, ONR contract N00014-86-K-0381, April 1990.

15. "Cyclic Stress-Strain Behavior of Titanium in the Presence of Porosity," (with D. Gerard) Tech. Report No. 15, ONR Contract N00014-86-K-0381, April 1990.

16. "Advanced Processing and Properties of High Performance Alloys" Technical Report No. 16, ONR Contract N00014-86-K-0381 April, 1990.

17. "Microstructures of Cu-Nb Alloys" (with K. Zeik and I. Anderson), Tech. Report No. 17, ONR Contract N00014-86-K-0381, July 1990.